LETTER

doi:10.1038/nature10974

Spin–orbital separation in the quasi-one-dimensional Mott insulator Sr_2CuO_3

J. Schlappa[1,2], K. Wohlfeld[3], K. J. Zhou[1]†, M. Mourigal[4], M. W. Haverkort[5], V. N. Strocov[1], L. Hozoi[3], C. Monney[1], S. Nishimoto[3], S. Singh[6]†, A. Revcolevschi[6], J.-S. Caux[7], L. Patthey[1,8], H. M. Rønnow[4], J. van den Brink[3] & T. Schmitt[1]

When viewed as an elementary particle, the electron has spin and charge. When binding to the atomic nucleus, it also acquires an angular momentum quantum number corresponding to the quantized atomic orbital it occupies. Even if electrons in solids form bands and delocalize from the nuclei, in Mott insulators they retain their three fundamental quantum numbers: spin, charge and orbital[1]. The hallmark of one-dimensional physics is a breaking up of the elementary electron into its separate degrees of freedom[2]. The separation of the electron into independent quasi-particles that carry either spin (spinons) or charge (holons) was first observed fifteen years ago[3]. Here we report observation of the separation of the orbital degree of freedom (orbiton) using resonant inelastic X-ray scattering on the one-dimensional Mott insulator Sr_2CuO_3. We resolve an orbiton separating itself from spinons and propagating through the lattice as a distinct quasi-particle with a substantial dispersion in energy over momentum, of about 0.2 electronvolts, over nearly one Brillouin zone.

It was pointed out in the 1970s that in a solid not only the charge and spin of electrons can become ordered—leading to magnetism—but also the electrons' orbital degree of freedom[1]. This observation sparked a field that has gone on to produce a number of important results. Although a physical electron combines spin, charge and orbital, theoretically an electron can be considered a bound state of the three independent, fundamental quasi-particles: a spinon, carrying the electron's spin; a holon (or chargon), carrying its charge; and an orbiton, carrying its orbital degree of freedom.

A remarkable and fundamental property of one-dimensional (1D) systems is that electronic excitations break up into deconfined spinons and holons. This was predicted decades ago (ref. 2 and references therein) and confirmed in the mid 1990s by angle-resolved photoemission spectroscopy experiments[3–5]. The spin–charge separation is an example of particle fractionalization, a phenomenon in which the quantum numbers of quasi-particles are not multiples of those of the elementary particle, but fractions. This effect is one of the most unusual manifestations of collective quantum physics of interacting particles and is a profound concept that has found its way into a number of theories, for example that describing high-temperature superconductivity in copper oxides[6,7].

To search for the further fractionalization of the electron, we consider the excitation of a copper orbital degree of freedom in the antiferromagnetic spin-chain compound Sr_2CuO_3. The spin–orbital separation process that we are looking for is analogous to the spin–charge separation mechanism (Fig. 1b). The latter occurs, for instance, when an electron is annihilated, removing a single spin and leaving behind a hole in the antiferromagnetic chain. This hole can start to propagate freely only after exciting one spinon (a domain wall in the antiferromagnetic chain). Subsequently, the spinon can delocalize and separate itself completely from the holon. When instead of creating a hole, as typically is done in a photoemission experiment, an electron is excited from one copper 3*d* orbital to another, the phenomenon of spin–orbital separation can in principle occur (Fig. 1a). The orbiton created in this manner may also deconfine after exciting a spinon, thus splitting the electron into its orbital and spin degrees of freedom[8].

Here we use high-resolution resonant inelastic X-ray scattering (RIXS) to search experimentally for spin–orbital separation in the quasi-1D copper oxide Sr_2CuO_3 (for material details, see Supplementary Information, section 1). We observe deconfinement of the spinon and orbiton during orbital excitation from the ground-state copper $3d\ x^2-y^2$ orbital to an excited copper $3d\ xy$ or xz orbital (Fig. 1c–e). For simplicity, we will from henceforth use the so-called 'hole' language: although nominally there are nine electrons in the 3*d* orbitals of the Cu^{2+} ion in Sr_2CuO_3, by using the 'electron–hole' transformation we can map the problem onto an effective system with one particle occupying a single 3*d* orbital (Supplementary Information, section 2).

We measure an orbiton dispersion that is almost as large as the dispersion of the two-spinon continuum at low energies. As for spin–charge separation[3–5], the orbiton dispersion has periodicity π (see Fig. 1c and see discussion below), which indicates the presence of an orbiton liberated from the spinon.

We measured the orbital excitations of Sr_2CuO_3 using RIXS at the L_3 edge of the copper ion. RIXS is a second-order scattering technique and can excite transitions between the copper 3*d* states of different symmetry (orbital excitations), owing to the involvement of two subsequent electric dipole transitions[9,10] (Supplementary Information, section 3). With the unique capability of RIXS also to probe spin excitations[11–13] and to vary the photon momentum transfer, the dispersion of orbital and spin excitations can be mapped out across the first Brillouin zone[11–16]. The experiments were carried out at the ADRESS beamline of the Swiss Light Source at the Paul Scherrer Institut[17,18].

For fixed momentum transfer, $\mathbf{q}$, along the chains, peaks in the RIXS spectrum at constant energy transfer reveal the presence of charge-neutral elementary excitations and are visible in the RIXS intensity map of Sr_2CuO_3 across the copper L_3 edge in Fig. 2a. The spectrum for which the incident energy was precisely tuned to the resonance maximum of the absorption spectrum is shown in Fig. 2b. In both plots, the excitations of the spin, orbital and charge degrees of freedom are indicated. The momentum dependence and, in particular, the dispersion of the spin and orbital excitations (Fig. 1c and Supplementary Fig. 2a) are indicative of their collective nature.

For energy transfers of up to ~0.8 eV purely magnetic excitations are present, but the spectrum between ~1.5 and ~3.5 eV corresponds to excitations from the copper $3d\ x^2-y^2$ ground state to orbitals of xy, xz/yz and $3z^2-r^2$ symmetry (Fig. 1d, e). These peaks correspond to

[1]Paul Scherrer Institut, Swiss Light Source, CH-5232 Villigen PSI, Switzerland. [2]Institut Methoden und Instrumentierung der Forschung mit Synchrotronstrahlung G-I2, Helmholtz-Zentrum Berlin für Materialien und Energie GmbH, D-12489 Berlin, Germany. [3]Institute for Theoretical Solid State Physics, IFW Dresden, Helmholtzstrasse 20, 01069 Dresden, Germany. [4]Ecole Polytechnique Fédérale de Lausanne, CH-1015 Lausanne, Switzerland. [5]Max Planck Institute for Solid State Research, D-70569 Stuttgart, Germany. [6]ICMMO - UMR 8182 - Bâtiment 410, Université Paris-Sud 11, 91405 Orsay Cedex, France. [7]Institute for Theoretical Physics, University of Amsterdam, Science Park 904, Postbus 94485, 1090 GL Amsterdam, The Netherlands. [8]SwissFEL, CH-5232 Villigen PSI, Switzerland. †Present addresses: Diamond Light Source, Harwell Science and Innovation Campus, Didcot, Oxfordshire OX11 0DE, UK (K.J.Z.); Indian Institute of Science Education and Research, 900 NCL Innovation Park, Pashan, 411008 Pune, India (S.S.).

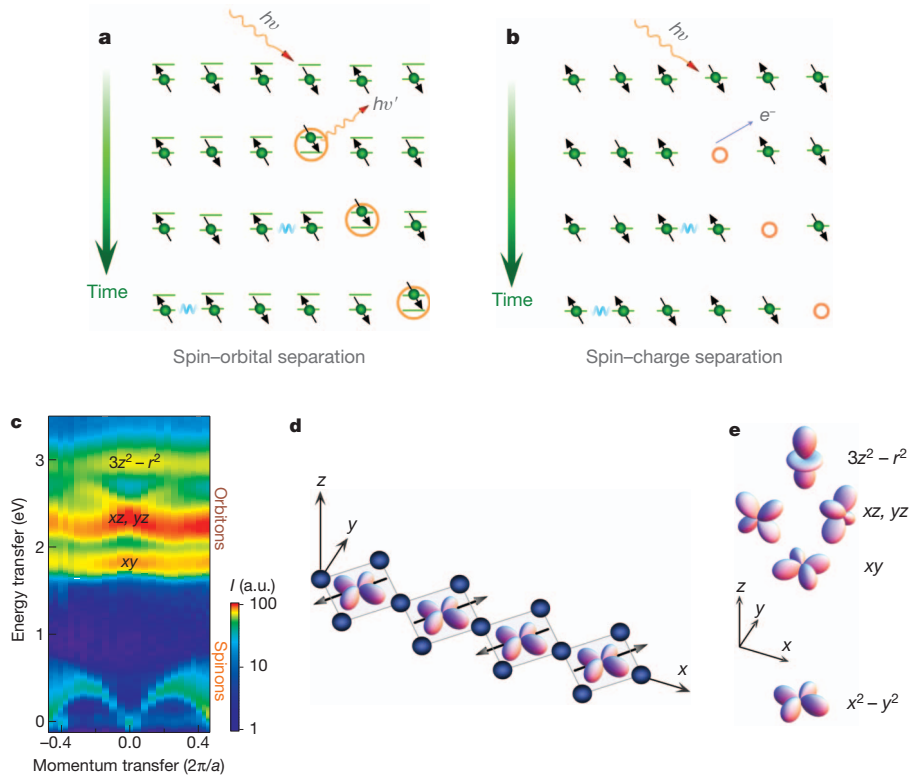

Figure 1 | Spin–orbital separation process in an antiferromagnetic spin chain, emerging after exciting an orbital. **a**, **b**, Sketches of spin–orbital separation (**a**) and spin–charge separation (**b**), generated in processes of RIXS and angle-resolved photoemission spectroscopy, respectively. The spin is represented by the arrow and the charge is represented by the green dot. In **a**, the lower and upper lines represent the ground-state and excited-state orbitals, respectively. **c**, RIXS intensity map of the dispersing spin and orbital excitations in Sr_2CuO_3 as functions of photon momentum transfer along the chains and photon energy transfer (for details, see main text and Supplementary Information, section 3). *a*, [100] lattice constant; a.u., arbitrary units. Data obtained at $\Psi = 130^\circ$. **d**, Geometry of the CuO_3 chain, with the ground-state copper $3d\ x^2 - y^2$ orbitals in the middle of each plaquette and oxygen sites at the plaquette corners. **e**, Orbital symmetries of $x^2 - y^2$ and excited $3d$ orbitals. In panels **c**–**e**, 'hole' language is used (Supplementary Information, section 2).

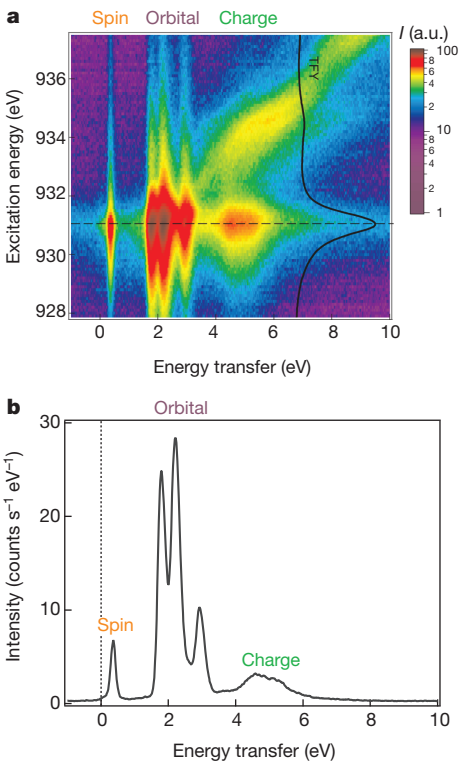

orbital excitations (called also *d*–*d* excitations), and not, for example, to charge transfer excitations, the intensity of which is non-zero for energies up to ~6 eV but here for the case of *L*-edge RIXS is at least an order of magnitude lower[10]. The orbital assignment of these excitations was unambiguously verified by comparing their energy at $\mathbf{q} = 0$ with *ab initio* quantum chemistry cluster calculations[19] (Supplementary Information, section 5, for detailed results).

Zooming into the 'magnetic' part of Fig. 1c, between 0 and 0.8 eV in energy transfer, reveals strongly dispersing spin excitations. At the lower boundary the dispersion has period π, and at the continuum (upper boundary) it has period 2π (Fig. 3a). These RIXS data agree very well with recent inelastic neutron scattering studies on Sr_2CuO_3 (ref. 20). The simultaneous presence in the spectrum of a lower edge with period π and an upper one with period 2π indicates directly that in the spin chain the magnetic excitations with spin 1 break up and fractionalize into two-spinon (and higher-order) excitations that make up a continuum[20], with each spinon having spin 1/2. These spectra confirm that RIXS for magnetic excitations probes the well-known spin dynamical structure factor as theoretically predicted[11–13], in agreement with recent studies on TiOCl (ref. 21). The excellent statistics of

Figure 2 | Energy dependence of elementary excitations in Sr_2CuO_3 observed with RIXS at the copper L_3-edge resonance. **a**, RIXS map of Sr_2CuO_3 (log scale) as a function of photon excitation energy (left axis) and energy transfer (bottom axis). The superimposed black curve shows the total fluorescence yield X-ray absorption spectrum. The dashed line marks the maximum energy of the copper L_3-edge resonance. **b**, RIXS line spectrum measured at the resonance maximum (along the dashed line in **a**). All data was obtained at a scattering angle of $\Psi = 90^\circ$ and for momentum transfer along the chain of $q = 0.189 \times 2\pi/a$ (Methods).

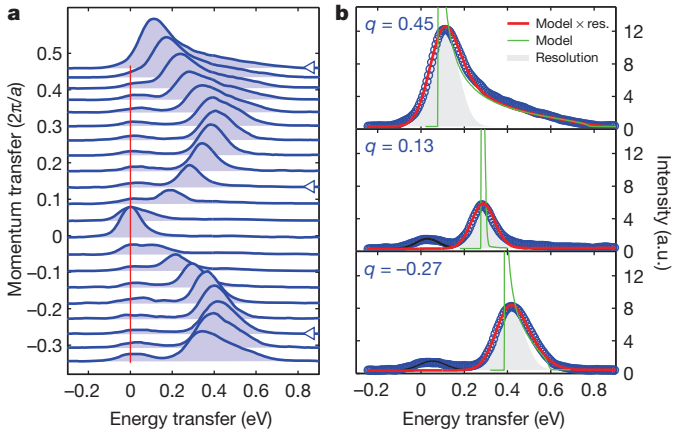

Figure 3 | Dispersion of magnetic excitations: experimental data and simulation. **a**, RIXS energy transfer spectra of the magnetic two-spinon continuum (see the spinon region in Fig. 1c). Data obtained at $\Psi = 130^{\circ}$. **b**, Fit (red line) of the experimental data (dots) with the two- and four-spinon dynamical structure factor[22] (green line), convolved with a Gaussian distribution (light-grey shaded region) to account for the total instrumental resolution of 140 meV. The low-energy peak at around 50 meV (black line) is elastic and phonon scattering. The values of momentum transfer for the selected spectra (shown in units of $2\pi/a$) are indicated by arrows in **a**.

the data further allow for a direct comparison of the RIXS line shapes with the exact two- and four-spinon dynamical structure factor of the spin-1/2 Heisenberg chain. In Fig. 3b, we show the fits for three selected momentum transfer values using the exact two- and four-spinon dynamical structure factor, $S(\mathbf{q}, \omega)$ (where $\mathbf{q}$ and ω stand for the momentum and energy of the created excitation, respectively) in the representation of ref. 22. The obtained exchange coupling, $J = 249$ meV, is in very good agreement with the value obtained from inelastic neutron scattering data[20].

Having unambiguously identified the fractionalized spinon excitations in the low-energy sector, we now concentrate on the orbital excitations spectrum in Fig. 4. We find that these are strongly momentum dependent and have a novel, distinct dispersion. This proves that the orbital excitations observed here are of collective nature. The *xz* excitation has the largest dispersion, of ~0.2 eV, and has a spectrum containing two peculiar components: a lower branch dispersing with periodicity π and, above that, an incoherent spectrum with a double-oval shape. This spectrum is strikingly similar to seemingly unrelated angle-resolved photoemission spectra of 1D copper oxides, which evidence spin–charge separation (see, for example, fig. 3 of ref. 3). This is an indication that the observed orbital dispersion is related to an analogous separation of degrees of freedom.

To test this conjecture, we derived a microscopic model that describes the spin–orbital interactions in Sr_2CuO_3 (Methods). The low-energy Kugel'–Khomskii Hamiltonian for this was obtained[8,23] from the charge transfer model of Sr_2CuO_3 in ref. 24. The crucial part of the Hamiltonian, responsible for the *xz* orbital propagation, is

$$H = -J_O \sum_{j,\sigma} (c^{+}_{j\sigma} c_{j+1,\sigma} + \text{h.c.}) + J \sum_j \mathbf{S}_j \cdot \mathbf{S}_{j+1} + E_O \sum_j (1 - n_j) \quad (1)$$

where J and J_O are respectively the spin and orbital exchange constants, both of which are fixed by the charge transfer model[24]; E_O is the *xz* orbital on-site energy; $c^{+}_{j\sigma}$ and $c_{j\sigma}$ are operators that respectively annihilate and create particles in *xz* orbital with spin σ; $\mathbf{S}_j$ is the spin of the particle in $x^2 - y^2$ orbital; $1 - n_j$ counts the number of particles in *xz* orbital; and 'h.c.' denotes Hermitian conjugate. The first term in the Hamiltonian describes the propagation of orbital excitations through the lattice. The second term represents the usual Heisenberg interaction between spins, which vanishes on bonds where an orbital excitation is present (Methods).

From purely a mathematical standpoint, equation (1) is identical to the 1D *t*–*J* model—describing the hopping of holes doped into an antiferromagnetic spin chain in which the spins interact via superexchange *J*—with the orbital superexchange, J_O, taking the place of *t*, the hole-hopping amplitude in the *t*–*J* model. This implies that the propagation of a single orbital excitation in the J_O–*J* model above is equivalent to the propagation of a single hole in the 1D *t*–*J* Hamiltonian. Because in the 1D *t*–*J* model a hole breaks up into a free spinon and holon, in the J_O–*J* model the orbital excitation will separate into a free spinon and orbiton.

Before calculating RIXS spectral functions and quantifying the separation of spin and orbital degrees of freedom in Sr_2CuO_3, it is instructive to consider the overall features of the momentum-dependent RIXS spectra within a slave-boson picture in terms of an orbital–spin separation ansatz. This ansatz is analogous to the mean-field slave-boson picture for charge–spin separation[25,26], which stipulates that the hole spectral function is given by the convolution of the spectral function of a free holon and a free spinon. In orbital–spin separation ansatz, free orbitons and spinons, created by the operators o^{+}_{i} and $s^{+}_{i\sigma}$, form the particle creation operator $c^{+}_{i\sigma} = s^{+}_{i\sigma} o_i$. On applying this formalism to the Hamiltonian in equation (1), the energies of non-interacting orbitons and spinons with momentum k become $\varepsilon_O(k) = E_O - 2J_O \cos(k)$ and $\varepsilon_S(k) = -J \cos(k)$, respectively. In this ansatz, the spectral function for the orbital excitation produced in RIXS, $c^{+}_{q\sigma} = \sum_k o_{q-k} s^{+}_{\sigma k}$ (where q, the x component of $\mathbf{q}$, is here the momentum transfer along the CuO_3 chain direction), is determined by a convolution of these two dispersions. The resulting excitation continuum is shown in Fig. 4b and has three defining features[25,26]: a prominent lower edge with energy, $E(q) = E_O - 2J_O|\sin(q)|$, that is entirely determined by the dispersion of the orbiton; a distinctive upper orbiton edge at $E(q) = E_O + 2J_O|\sin(q)|$; and a broader upper limit of the orbiton–spinon continuum at $F(q) = E_O + \sqrt{J^2 + 4J_O^2 - 4JJ_O \cos(q)}$. These dispersion curves are directly compared to our RIXS experiments in

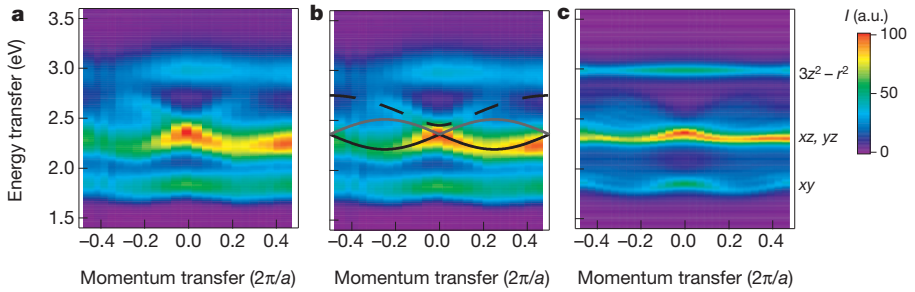

Figure 4 | Dispersion of orbital excitations: comparison between experiment and *ab initio* calculations. **a**, **c**, Comparison between the orbital region in Fig. 1c (**a**, left) and theory, using the J_O–*J* model (**c**, right). **b**, Lower and upper edges of the orbiton dispersion (solid black and grey lines) and the upper edge of the spinon–orbiton continuum (dashed line), as calculated using the orbital–spin separation ansatz. See main text and Supplementary Information for further details.

Fig. 4b. The measured spectral weight that accumulates at the first two lower-energy features does so with periodicity π, which is a direct consequence of spin–orbital separation.

To quantify the spectral weights within the orbiton–spinon continuum, we have calculated for the J_O–J Hamiltonian the orbital excitation Green's function by exactly diagonalizing the Hamiltonian on 28 lattice sites (as in the spin–charge separation studies[3], finite-size effects are negligible (they are estimated at ~0.01 eV)). From this, we calculate the RIXS spectrum following ref. 13, that is, by expressing the RIXS amplitude as a product of the single-ion local RIXS effective operator and the orbital excitation Green's function (Methods).

We find excellent agreement between theory and experiment (Fig. 4): both the sine-like *xz* orbiton dispersion and the *xz* spinon–orbiton continuum (the 'double-oval' incoherent spectrum), which are the hallmarks of spin–orbital separation, are present in the theory. The calculations also show that, in contrast to the *xz* orbital, the *xy* orbital has a small dispersion and that the excitations of both the $3z^2 - r^2$ orbital and the *yz* orbital are dispersionless, as is observed experimentally. This is an independent merit of the model because no fitting of dispersions to experimental data is involved.

The large orbiton dispersion observed in this study is the key feature that distinguishes Sr_2CuO_3 from other systems with orbital excitations[27–29], and relies on the 1D character of Sr_2CuO_3. In a system of higher dimensionality, orbitons interact with magnetic excitations, which tend to slow them down and thus reduce their dispersion. In one dimension, orbitons can avoid these renormalization effects by means of spin–orbital separation.

METHODS SUMMARY

We applied the technique of high-resolution RIXS with the incident photon energy tuned to the L_3 edge ($2p_{3/2} \rightarrow 3d$ resonance) of the copper ion (around 931 eV) and a total experimental resolution of 140 meV. The experiments were performed at the ADRESS beamline of the Swiss Light Source at the Paul Scherrer Institut[17,18]. The RIXS spectrometer was located at a fixed scattering angle of either $\Psi = 90^\circ$ or 130° and was collecting signal within the solid angle of (19.3×3.3) mrad^2 (horizontal × vertical detection direction; for a sketch of the experimental geometry, see Supplementary Fig. 1).

Single-crystal samples of Sr_2CuO_3 were grown by the floating-zone method and freshly cleaved before the RIXS experiment. The surface normal to the sample, [010], and the propagation direction of the chains, [100], were oriented parallel to the scattering plane. The sample was cooled with a helium-flow cryostat to 14 K during the measurements. Incident photons were linearly polarized in the scattering plane (π-orientation). The momentum transfer along the chains, q, was varied by changing the incidence angle in steps of $5 \pm 1^\circ$.

Theoretical modelling was done by deriving a Kugel'–Khomskii Hamiltonian from the charge transfer model and then writing it in a representation similar to the one used for the t–J model. Using this model, we calculated the spectral functions for the case of a single orbital excitation in the antiferromagnetic background by solving the Hamiltonian numerically on 28 sites. Such calculations were repeated separately for the two distinct dispersive orbital excitations, whereas for the non-dispersive excitations we confirmed that the parameters of the model did not allow for a dispersion larger than the experimental resolution. Finally, the RIXS cross-section was calculated by multiplying the calculated spectral functions for the orbital excitations by the local RIXS form factors.

Full Methods and any associated references are available in the online version of the paper at www.nature.com/nature.

Received 28 September 2011; accepted 17 February 2012.
Published online 18 April; corrected 2 May 2012 (see full-text HTML version for details).

1. Kugel', K. I. & Khomskii, D. I. The Jahn-Teller effect and magnetism: transition metal compounds. *Sov. Phys. Usp.* **25,** 231–256 (1982).
2. Giamarchi, T. *Quantum Physics in One Dimension* (Clarendon Press, 2004).
3. Kim, C. *et al.* Observation of spin-charge separation in one-dimensional $SrCuO_2$. *Phys. Rev. Lett.* **77,** 4054–4057 (1996).
4. Fujisawa, H. *et al.* Angle-resolved photoemission study of Sr_2CuO_3. *Phys. Rev. B* **59,** 7358–7361 (1999).
5. Kim, B. J. *et al.* Distinct spinon and holon dispersions in photoemission spectral functions from one-dimensional $SrCuO_2$. *Nature Phys.* **2,** 397–401 (2006).
6. Anderson, P. W. The resonating valence bond state in La_2CuO_4 and superconductivity. *Science* **235,** 1196–1198 (1987).
7. Senthil, T. & Fisher, M. P. A. Fractionalization in the cuprates: detecting the topological order. *Phys. Rev. Lett.* **86,** 292–295 (2001).
8. Wohlfeld, K., Daghofer, M., Nishimoto, S., Khaliullin, G. & van den Brink, J. Intrinsic coupling of orbital excitations to spin fluctuations in Mott insulators. *Phys. Rev. Lett.* **107,** 147201 (2011).
9. Ament, L., van Veenendaal, M., Devereaux, T., Hill, J. P. & van den Brink, J. Resonant inelastic X-ray scattering studies of elementary excitations. *Rev. Mod. Phys.* **83,** 705–767 (2011).
10. Moretti Sala, M. *et al.* Energy and symmetry of dd excitations in undoped layered cuprates measured by Cu L_3 resonant inelastic x-ray scattering. *N. J. Phys.* **13,** 043026 (2011).
11. Ament, L. J. P., Ghiringhelli, G., Moretti Sala, M., Braicovich, L., &. van den Brink, J. Theoretical demonstration of how the dispersion of magnetic excitations in cuprate compounds can be determined using resonant inelastic x-ray scattering. *Phys. Rev. Lett.* **103,** 117003 (2009).
12. Luo, J., Trammell, G. T. & Hannon, J. P. Scattering operator for elastic and inelastic resonant x-ray scattering. *Phys. Rev. Lett.* **71,** 287–290 (1993).
13. Haverkort, M. W. Theory of resonant inelastic X-ray scattering by collective magnetic excitations. *Phys. Rev. Lett.* **105,** 167404 (2010).
14. Schlappa, J. *et al.* Collective magnetic excitations in the spin ladder $Sr_{14}Cu_{24}O_{41}$ Measured using high-resolution resonant inelastic X-Ray scattering. *Phys. Rev. Lett.* **103,** 047401 (2009).
15. Braicovich, L. *et al.* Magnetic excitations and phase separation in the underdoped $La_{2-x}Sr_xCuO_4$ superconductor measured by resonant inelastic X-ray scattering. *Phys. Rev. Lett.* **104,** 077002 (2010).
16. Le Tacon, M. *et al.* Intense paramagnon excitations in a large family of high-temperature superconductors. *Nature Phys.* **7,** 725–730 (2011).
17. Strocov, V. N. *et al.* High-resolution soft X-ray beamline ADRESS at the Swiss Light Source for resonant inelastic X-ray scattering and angle-resolved photoelectron spectroscopies. *J. Synchrotron Radiat.* **17,** 631–643 (2010).
18. Ghiringhelli, G. *et al.* SAXES, a high resolution spectrometer for resonant x-ray emission in the 400–1600 eV energy range. *Rev. Sci. Instrum.* **77,** 113108 (2006).
19. Hozoi, L., Siurakshina, L., Fulde, P. & van den Brink, J. Ab initio determination of Cu 3d orbital energies in layered copper oxides. *Sci. Rep.* **1,** 1–4 (2011).
20. Walters, A. C. *et al.* Effect of covalent bonding on magnetism and the missing neutron intensity in copper oxide compounds. *Nature Phys.* **5,** 867–872 (2009).
21. Glawion, S. *et al.* Two-spinon and orbital excitations of the spin-Peierls system TiOCl. *Phys. Rev. Lett.* **107,** 107402 (2011).
22. Caux, J.-S. & Hagemans, R. The four-spinon dynamical structure factor of the Heisenberg chain. *J. Stat. Mech.* **2006,** P12013 (2006).
23. Oleś, A. M., Khaliullin, G., Horsch, P. & Feiner, L. F. Fingerprints of spin-orbital physics in cubic Mott insulators: magnetic exchange interactions and optical spectral weights. *Phys. Rev. B* **72,** 214431 (2005).
24. Neudert, R. *et al.* Four-band extended Hubbard Hamiltonian for the one-dimensional cuprate Sr_2CuO_3: distribution of oxygen holes and its relation to strong intersite Coulomb interaction. *Phys. Rev. B* **62,** 10752–10765 (2000).
25. Brunner, M. Assaad, F. F. & Muramatsu, A. Single hole dynamics in the one dimensional t-J model. *Eur. Phys. J. B* **16,** 209–212 (2000).
26. Suzuura, H. & Nagaosa, N. Spin-charge separation in angle-resolved photoemission spectra. *Phys. Rev. B* **56,** 3548–3551 (1997).
27. Macfarlane, R. M. & Allen, J. W. Exciton bands in antiferromagnetic Cr_2O_3. *Phys. Rev. B* **4,** 3054–3067 (1971).
28. Grüninger, M. *et al.* Experimental quest for orbital waves. *Nature* **418,** 39–40 (2002).
29. Ulrich, C. *et al.* Momentum dependence of orbital excitations in Mott-insulating titanates. *Phys. Rev. Lett.* **103,** 107205 (2009).

Supplementary Information is linked to the online version of the paper at www.nature.com/nature.

Acknowledgements This work was performed at the ADRESS beamline of the Swiss Light Source using the SAXES instrument jointly built by the Paul Scherrer Institut, Switzerland, and Politecnico di Milano, Italy. We acknowledge support from the Swiss National Science Foundation and its NCCR MaNEP. K.W. acknowledges support from the Alexander von Humboldt foundation and discussions with M. Daghofer and S.-L. Drechsler. J.-S.C. acknowledges support from the Foundation for Fundamental Research on Matter and from the Netherlands Organisation for Scientific Research. S.S. and A.R. acknowledge the support of the European contract NOVMAG. This research benefited from the RIXS collaboration supported by the Computational Materials Science Network programme of the Division of Materials Science and Engineering, US Department of Energy, grant no. DE-SC0007091.

Author Contributions J.S., T.S. and H.M.R. planned the experiment. S.S. and A.R. fabricated the samples. J.S., K.J.Z., V.N.S. and T.S. carried out the experiment. J.S. and M.M. carried out the data analysis. C.M. helped with the data analysis. K.W. and J.v.d.B. developed the theory for the spin–orbital separation with assistance from M.W.H., L.H. and S.N. J.-S.C. provided the theory for the spin excitations. J.S., K.W., K.J.Z., H.M.R., J.v.d.B. and T.S. wrote the paper with contributions from all co-authors. L.P., H.M.R., J.v.d.B. and T.S. supervised the project.

Author Information Reprints and permissions information is available at www.nature.com/reprints. The authors declare no competing financial interests. Readers are welcome to comment on the online version of this article at www.nature.com/nature. Correspondence and requests for materials should be addressed to J.S. (justine.schlappa@helmholtz-berlin.de) or T.S. (thorsten.schmitt@psi.ch).

METHODS

Experiment. We applied the technique of high-resolution RIXS with the incident photon energy tuned to the L_3 edge ($2p_{3/2} \rightarrow 3d$ resonance) of the copper ion (around 931 eV) and a total experimental resolution of 140 meV. The experiments were performed at the ADRESS beamline of the Swiss Light Source at the Paul Scherrer Institut[17,18]. Single-crystal samples of Sr_2CuO_3 were grown by the floating-zone method and freshly cleaved before the experiment. The samples were mounted such that the surface normal, [010], and the chain propagation direction, [100], were oriented parallel to the scattering plane (Supplementary Information, section 4, and Supplementary Fig. 1). The polarization vector of the incident light, $\boldsymbol{\varepsilon}_{in}$, was parallel to the scattering plane (π-orientation). This yielded the maximum cross-section for the copper $2p^63d^9 \rightarrow 2p^53d^{10}$ transition. The RIXS spectrometer was located at a fixed scattering angle of either $\Psi = 90^\circ$ or 130°, collecting signal within a solid angle of (19.3×3.3) mrad^2 (horizontal $\times$ vertical detection direction). The momentum transfer along the chains, q, was varied by changing the incidence angle in steps of $5 \pm 1^\circ$. This results in the RIXS signal being polarization dependent and the relative intensity of the orbital excitations varying as a function of q. (For details on the polarization dependence of the orbital excitations, see the discussion of the RIXS cross-section below.) Supplementary Fig. 2a shows the RIXS line spectra, which correspond to the intensity map data in Fig. 1c, and Supplementary Fig. 2b shows the variation in the polarization of the incident photons with q. We estimate the systematic errors in the momentum transfer to be about $0.006 \times 2\pi/a$ and $0.013 \times 2\pi/a$ at the edge and the centre of the Brillouin zone, respectively. The error in determining the energy zero of the energy transfer scale is about 30 meV. The sample was cooled with a helium-flow cryostat to 14 K during the measurements.

Theory of spin excitations. Owing to the particular choice of the experimental geometry, the RIXS cross-section for spin excitations (that is, the magnetic part of the spectrum extending up to $\sim$0.8 eV) is directly proportional to the two-point dynamical spin–spin correlation function (local RIXS form factors are independent of transferred momentum here); see refs 9, 11–14. Therefore, the magnetic part of the RIXS spectrum was fitted to the two-point dynamical spin–spin correlation function (see below), convolved with a Gaussian to account for experimental resolution and adding a low-energy Gaussian covering the elastic and phonon peak around 50 meV. This captured most of the measured intensity with nearly constant J, amplitude and resolution. Fixing these three parameters to their mean values gives reasonable fits for all q. The time-normalized data sets were corrected for the effective scattering volume, V_{eff}:

$$\frac{1}{V_{eff}} = 1 + \frac{\mu_1}{\mu_2}(\omega)\frac{\sin(\theta)}{\sin(\beta)}(q)$$

Here $(\sin(\theta)/\sin(\beta))(q)$ is a geometric term, θ and β being the angles between the sample surface and the direction of photon incidence and, respectively, the direction of photon detection; and $(\mu_1/\mu_2)(\omega)$ is an outgoing-energy-dependent absorption factor derived from the total fluorescence yield X-ray absorption spectra.

The exact solvability of the Heisenberg spin-1/2 chain is exploited to compute its two-point dynamical spin–spin correlation function. At zero magnetization, this is predominantly carried by two- and four-spinon intermediate states whose exact contributions can be written in the thermodynamic limit in terms of fundamental integrals by using the vertex operator approach[22]. The numerical evaluation of these integrals provides the dynamical structure factor throughout the Brillouin zone, yielding sum-rule saturations of the order of 98%.

Theory of orbital excitations. We first calculate the energies of the 3d orbitals in Sr_2CuO_3 using the *ab initio* quantum chemistry method (Supplementary Information, section 5). Although this method is not tailored to calculate the dispersion of orbital excitations (for which model calculations are needed) owing to the finite size of the cluster, it identifies from first principles the energies of orbital excitations in Sr_2CuO_3 for $\mathbf{q} = \mathbf{0}$ transferred momentum. These energies have been found to be in close agreement with both optical absorption and RIXS experiments[19]. Owing to the large separation of the d–d excitations energies (Supplementary Table 1), we can separately model the momentum-dependent RIXS cross-section for each orbital excitation for the case of non-negligible inter-orbital hopping. For this (see the next section), the Kugel'–Khomskii Hamiltonian for the case of a single orbital excitation (for example the $x^2 - y^2 \rightarrow xz$ transition) from a ferro-orbital ground state (that is, one in which all $x^2 - y^2$ orbitals are occupied) is derived on the basis of the established charge transfer model for Sr_2CuO_3. Similar calculations are performed for the other orbital excitation symmetries (see the next section) and the RIXS cross-section based on the solution to these model calculations is calculated (see the discussion of RIXS cross-section below).

Model Hamiltonian. In Mott insulators, the Kugel'–Khomskii model is the effective low-energy superexchange model for coupled spin and orbital excitations; compare with ref. 1. We first consider only an xz orbital excitation, which may hop between the copper sites in a 'three-step' perturbative superexchange process with an energy scale $\sim t_1 t_2/2U$. First the particle in the excited orbital moves from site j to the neighbouring site $j+1$ by hopping with amplitude $\sim t_2$; next an intermediate state, in which two particles are on site $j+1$ and which has an energetic cost equivalent to the on-site Coulomb repulsion $\sim U$, is formed; and finally the particle in the ground-state orbital moves from site $j+1$ to site j by hopping with amplitude t_1. Thus, we obtain

$$H_O = -J_O \sum_{j,\sigma} (c^+_{j\sigma} c_{j+1,\sigma} + \text{h.c.}) + E_O \sum_j (1 - n_j) \qquad (2)$$

where $J_O = (3R_1 + R_2)2t_1t_2/U$ and E_O is the energy cost of the orbital excitation. In J_O, $R_1 = 1/(1-3\eta)$ and $R_2 = 1/(1-\eta)$ originate in the multiplet structure of the intermediate states of the superexchange processes and depend on the ratio, $\eta = J_H/U$, of the Hund's exchange to the Coulomb repulsion. Although the above equation is given for the Mott–Hubbard limit of the superexchange model, in our calculation we modified the parameters to account for superexchange processes on oxygen atoms in Sr_2CuO_3. For a standard set of charge transfer parameters[24], this gives $J_O \approx 0.075$ eV without any fitting to the experimental data. The values of E_O are determined from the RIXS experiment and are within 10% of the on-site orbital energies obtained using *ab initio* quantum chemistry cluster calculations[19] for four CuO_4 plaquettes in Sr_2CuO_3 (Supplementary Information, section 5).

In equation (2), $c_{j\sigma}$ is a fermion operator, acting in the restricted Hilbert space with no double occupancies, that creates an orbital excitation (a hole in the spin background in the language of the t–J model) at site j with spin σ, and $1 - n_j = 1 - \sum_\sigma c^+_{j\sigma} c_{j\sigma}$ is the number operator that counts the number of orbital excitations in the chain. Note that this 'fermionization' of the 1D problem was performed by replacing the standard orbital pseudospin operators[23] with fermions by Jordan–Wigner transformation (see ref. 8 for details).

The second part of the Hamiltonian in equation (1) corresponds to the spin dynamics on the bonds where the orbital excitation is not present:

$$H_S = J \sum_j \mathbf{S}_j \cdot \mathbf{S}_{j+1}$$

Here $J = 4t_1^2/U$ is now the well-known Heisenberg antiferromagnetic superexchange constant. In sum, H_S and H_O constitute the Hamiltonian H from equation (1).

Excitations from the ground-state $3d\ x^2 - y^2$ orbital to either the xy orbital or the xz orbital are described by H, but with different effective parameters because the hopping amplitudes from each of these orbitals to the neighbouring bonding oxygen orbitals and, subsequently, to the neighbouring copper sites differ. In particular, for the xy orbital the effective hopping amplitude along the chain is $\sim$25% smaller than that for the xz orbital owing to the formation of bonding and antibonding states with 2p orbitals on oxygen atoms outside the copper–oxygen chain. For orbital excitations involving the yz and $3z^2 - r^2$ orbitals, the dispersion vanishes because the hopping matrix elements to the neighbouring oxygen orbitals along the chain are either much smaller than for the xy or xz orbital excitations ($3z^2 - r^2$ orbital) or are vanishingly small[24] (yz orbital).

RIXS cross-section. Local effective RIXS operators have been derived for the Cu^{2+} ($3d^9$) electronic configuration[12,30] (see also Supplementary Information, section 3). However, several simplifications beyond the local effective scattering operators as used in refs 12–13, 30 are justified, because the spin of the particle in the excited orbital is to a good approximation conserved (Hund's exchange is one order of magnitude smaller than the on-site Coulomb repulsion[23,24] during orbiton propagation). First, the spectrum obtained is independent of the spin of the particle in the excited orbital. Second, the spin and the orbital character of the excited particle are conserved during propagation. The RIXS intensity for an orbital excitation is therefore given by the sum of the intensities for scattering from initial states with spin up or down to final states with the spin either flipped or conserved. This allows us to express the RIXS intensity as the product[11,13] of polarization-dependent intensities and the non-local dynamical structure factor $O(q,\omega)$, which is defined as the spectral function of the single orbital excitation created using operator $c_{j\sigma}$ and propagating with Hamiltonian H (ref. 8). This structure factor is either equal to one, for 'non-dispersive' orbital excitations ($3z^2 - r^2$ and yz orbitals; see previous section), or is calculated numerically by exactly solving the Hamiltonian H on a finite chain of 28 sites. The latter is done separately for xz and xy orbital excitations. We note that such a separation is possible because orbiton–orbiton interactions vanish for one-orbiton excitations in the chain. The results of these calculations are presented in Fig. 4c.

30. van Veenendaal, M. Polarization dependence of L- and M-edge resonant inelastic X-ray scattering in transition-metal compound. *Phys. Rev. Lett.* **96,** 117404 (2006).